Large Magnetoresistance in an Electric-Field-Controlled Antiferromagnetic Tunnel Junction

Yurong Su,[1] Jia Zhang,[2,*] Jing-Tao Lü,[2] Jeongmin Hong,[1] and Long You[1,†]

[1] *School of Optical and Electronic Information, Huazhong University of Science and Technology, 430074 Wuhan, China*

[2] *School of Physics and Wuhan National High Magnetic Field Center, Huazhong University of Science and Technology, 430074 Wuhan, China*

(Received 22 March 2019; revised manuscript received 28 August 2019; published 16 October 2019)

A large magnetoresistance effect controlled by an electric field rather than a magnetic field or electric current is a preferable routine for designing low-power-consumption magnetoresistance-based spintronic devices. We propose an electric-field-controlled antiferromagnetic (AFM) tunnel junction with the structure of the piezoelectric substrate/$Mn_3Pt/SrTiO_3/Pt$ operating by the magnetic phase transition (MPT) of antiferromagnet Mn_3Pt through its magneto-volume effect. The transport properties of the proposed AFM tunnel junction are investigated by employing first-principles calculations. Our results show that a magnetoresistance over hundreds of percentages is achievable when Mn_3Pt undergoes MPT from a collinear AFM state to a noncollinear AFM state. Band structure analysis based on density functional calculations shows that the large tunnel magnetoresistance can be attributed to the joint effect of significantly different Fermi surfaces of Mn_3Pt at two AFM phases and the band symmetry filtering effect of the $SrTiO_3$ tunnel barrier. In addition, other than the single-crystalline tunnel barrier, we also discuss the robustness of the proposed magnetoresistance effect by considering an amorphous AlO_x barrier. Our results may open a way for effective electrical writing and reading of the AFM state and its application in energy efficient magnetic memory devices.

DOI: 10.1103/PhysRevApplied.12.044036

I. INTRODUCTION

A conventional magnetic tunnel junction (MTJ) with high tunnel magnetoresistance (TMR) consists of two ferromagnetic (FM) electrodes separated by an ultrathin insulating barrier. The TMR effect can be applied in various spintronic devices, for instance, magnetoresistive random access memories (MRAM), magnetic field sensors, read heads for hard drives, and spin logics [1–3]. At the current stage, electric current has been mainly used to manipulate the magnetization states in MTJs via spin-transfer-torque (STT) [4–6], spin-orbit torque [7–9] mechanisms, or magnetic fields produced by current, which limits the energy efficiency of MTJ-based spintronic devices. Therefore, there have been great efforts aimed at electric field control of magnetic states instead of the electric current. Voltage-controlled magnetic anisotropy (VCMA) in a perpendicularly magnetized CoFe(B)/MgO interface is one of the promising strategies [10–13]. However, the VCMA effect mainly relies on the electrostatic screening of magnetic electrodes at the interface, and the voltage-controlled effect alone is not sufficient for effectively manipulating the magnetization state [10]. An alternative strategy toward electric field control of TMR is to use a ferroelectric barrier in a tunnel junction [14–16]. However, one of the main disadvantages of the ferroelectric tunnel junctions (FTJs) is the high resistance-area product due to the existence of the critical thickness for the ferroelectric polarization of the tunnel barrier [17].

Recently, an alternative route to obtain a moderate TMR has been proposed via the magnetic phase transition (MPT) of a magnetic electrode [18,19]. A typical structure of this type of MTJ might be a sandwich structure of "metallic MPT-electrode/insulating tunnel barrier/nonmagnetic metallic electrode." The magnetoresistance will arise when the internal magnetic structure of the MPT electrode changes with an external magnetic field, temperature, and so on. For instance, the α'-FeRh electrode can be switched from a *G* type antiferromagnetic (AFM) to a FM state via a magnetic field (on the order of several Tesla), and over 20% TMR at room temperature has been experimentally demonstrated in α'-FeRh/MgO/γ-FeRh MTJ [18]. In the present work, we will focus on another more attractive metallic AFM MPT material, Mn_3Pt, and discuss the corresponding magnetoresistance effect.

As a well-studied MPT material, the ground magnetic state of cubic Mn_3Pt is triangular noncollinear AFM (*D*

*jiazhang@hust.edu.cn
†lyou@hust.edu.cn

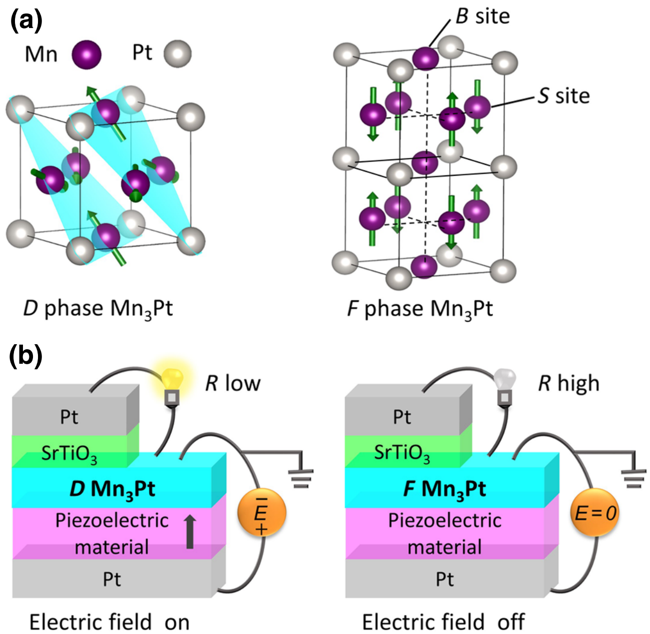

FIG. 1. (a) The illustrations of the atomic and magnetic structures of AFM Mn_3Pt in *D* and *F* phases. The Pt atoms are in gray and the Mn atoms are in purple. The green arrows indicate the magnetic moment directions on Mn atoms. (b) The demonstration and operation principles of an electric-field-driven MPT TMR effect in a tunnel junction with a Mn_3Pt electrode.

phase). It shows a first-order magnetic transition from the *D* phase to the collinear AFM state (*F* phase) when the temperature rises up to $T_{tr} \sim 365$ K [20,21], and it further becomes paramagnetic when the temperature is over $T_N \sim 475$ K. The magnetic structures of the two stable AFM states in bulk Mn_3Pt are illustrated in Fig. 1(a). The noncollinear *D* phase state with the magnetic moments of the three Mn atoms in the unit cell establish a triangular arrangement within the (111) plane. The *F* phase is a collinear magnetic structure with a doubled unit cell along the *c* direction.

What is more interesting, recent experiments demonstrate that being grown on a ferroelectric $BaTiO_3$ substrate, the transition temperature of Mn_3Pt can be shifted upward by applying an electric field through the $BaTiO_3$ substrate. Hence, the collinear *F* phase of Mn_3Pt can be driven into a noncollinear *D* phase by applying an electric field on a piezoelectric $BaTiO_3$ substrate above room temperature [22]. Therefore, it would be possible to design tunnel junctions by employing such an electric-field-controlled MPT of Mn_3Pt as is shown in Fig. 1(b). On the other hand, AFM materials are believed to be promising for applications in spintronic devices. However, the lack of an efficient method for electrical control of AFM states is one of the main obstacles for their applications in magnetic memory devices. Therefore, the possibility of designing the electric-field-controlled AFM Mn_3Pt-based tunnel junctions with large TMRs above room temperature may provide an alternative avenue for AFM spintronics [23,24].

We will first briefly discuss the mechanism of an electric-field-controlled MPT of Mn_3Pt on a piezoelectric substrate. The transition temperature T_{tr} of Mn_3Pt between the *D* and *F* phases has been found to be closely related to its lattice constant [25] due to the so-called "magnetovolume" effect [26]. The smaller lattice constant will result in a higher transition temperature T_{tr} of Mn_3Pt. When Mn_3Pt is grown on a piezoelectric substrate, for instance, $BaTiO_3$, the applied electric field across $BaTiO_3$ will lead to the decrease of the in-plane lattice constant due to the inverse piezoelectric effect, and correspondingly, the MPT temperature of Mn_3Pt will shift to a higher value. As a consequence, the electric field can be applied to switch the magnetic phase of Mn_3Pt between the collinear *F* phase and the noncollinear *D* phase at a certain temperature window as has been demonstrated experimentally [22].

A realistic Mn_3Pt-based AFM junction structure and its electric-field-driven operation principle is shown in Fig. 1(b). The whole $Mn_3Pt/SrTiO_3/Pt$ tunnel junction can be grown on a piezoelectric substrate, for example, $BaTiO_3$. The electric field is applied between the $BaTiO_3$ substrate and Mn_3Pt to write the AFM state of Mn_3Pt, and the tunnel resistance is measured between Mn_3Pt and the Pt electrode across the $SrTiO_3$ tunnel barrier. By comparing with conventional MTJs and FTJs, the advantages of the proposed tunnel junctions are multifold, including: (1) The magnetic phase of Mn_3Pt is controlled by an electric field rather than a magnetic field or electric current. In consequence, the proposed AFM MTJs may be more energy efficient in magnetoresistance-based memory devices. (2) The magnetoresistance is originating from the MPT of the Mn_3Pt electrode and a large TMR is possible. A high TMR of the tunnel junctions will then be beneficial to its application in a memory device with a high *on-off* ratio. (3) The electric-field-controlled MPT is switched between two AFM phases, and the whole tunnel junction might be robust against the external magnetic field perturbation and suitable for high-density nonvolatile memory. (4) The proposed tunnel junction structure is simple with only one magnetic electrode and the switching speed should be fast due to the AFM phase transition.

The remaining key issue of the proposed AFM tunnel junction will then be the spin-dependent transport properties, especially the conductance (resistance) ratio of the tunnel junction when Mn_3Pt is in the *F* and *D* phases, which is the main focus of the present work. In the past, there were also several experiments focusing on AFM tunnel junctions by using a collinear antiferromagnet $L1_0$-IrMn [27,28] or $L1_0$-MnPt [29] as an electrode. However, the magnetoresistances in those tunnel junctions, which originate from the anisotropic electronic structure of antiferromagnets, are relatively low (typically less than 10%). Hereafter, we will investigate the transport and the corresponding MPT TMR effect in a $Mn_3Pt/SrTiO_3/Pt$ tunnel junction through first-principles calculations.

II. CALCULATION METHODS

Experimentally, a Mn_3Pt film originally in the collinear F phase with $a = 3.875$ Å and $c = 3.850$ Å can be switched to the noncollinear D phase with $a = 3.866$ Å and $c = 3.860$ Å above room temperature by applying a moderate out-of-plane electric field $E = 4$ kV cm^{-1} [22]. The corresponding experimental lattice constants of Mn_3Pt for two magnetic phases are used in the present first-principles calculations. All the calculations in the present work are performed by employing the Quantum Espresso package [30] with the PBE GGA (Perdew-Burke-Ernzerhof type of generalized-gradient-approximation) exchange correlation potential [31] and ultrasoft pseudopotential [32] generated from PSlib0.3.1. A Monkhorst-Pack k point mesh of $16 \times 16 \times 16$ and a plane-wave cutoff of 50 Ry are adopted for the self-consistent electronic structure calculations of bulk Mn_3Pt. The calculated ground state of bulk Mn_3Pt is the D phase, which has a total energy 1.01 eV per formula cell lower than that of the F phase, which agrees with the previous theoretical value [33]. The magnetic moment on a Mn atom of the D phase is 3.10 μ_B and it agrees well with the experimental value of 3.0 μ_B [20,21]. For the F phase, the Mn spins on the S sites are 2.92 μ_B per Mn atom and on the B sites are nonzero, but have a small value of 0.11 μ_B along the c axis, resulting in a net magnetic moment and magnetization accordingly.

In order to calculate the electron transmission of the $Mn_3Pt/SrTiO_3/Pt$ tunnel junction, first, the electronic structures of the left Mn_3Pt electrode, the right Pt electrode, and the junction region in a $Mn_3Pt/SrTiO_3/Pt$ supercell are separately and self-consistently calculated. Then, the electron transmission is calculated by using a standard wave-function scattering method [32,34] in two-dimensional Brillouin zones (2DBZs) by matching the wave functions between the left and right electrodes. The ballistic Landauer conductance of the tunnel junction is calculated by summarizing the transmission over 200×200 $k_{||} = (k_x, k_y)$ points in 2DBZ:$G = (e^2/h) \sum_{k_{||}} T(k_{||})$, where $T(k_{||})$ is the k resolved transmission, e is the elementary charge, and h is the Plank constant.

III. RESULTS AND DISCUSSIONS

The Fermi surface (FS) of the electrode indicates the available Bloch states distributed over the Brillouin zone for electron transmission, and it is crucial for electron transport of MTJs. Figure 2(a) shows the side and top views (along the k_z direction) of the three-dimensional FSs for bulk Mn_3Pt in the D and F phases. Both AFM phases have multiple bands which are distributed over the 2DBZ,

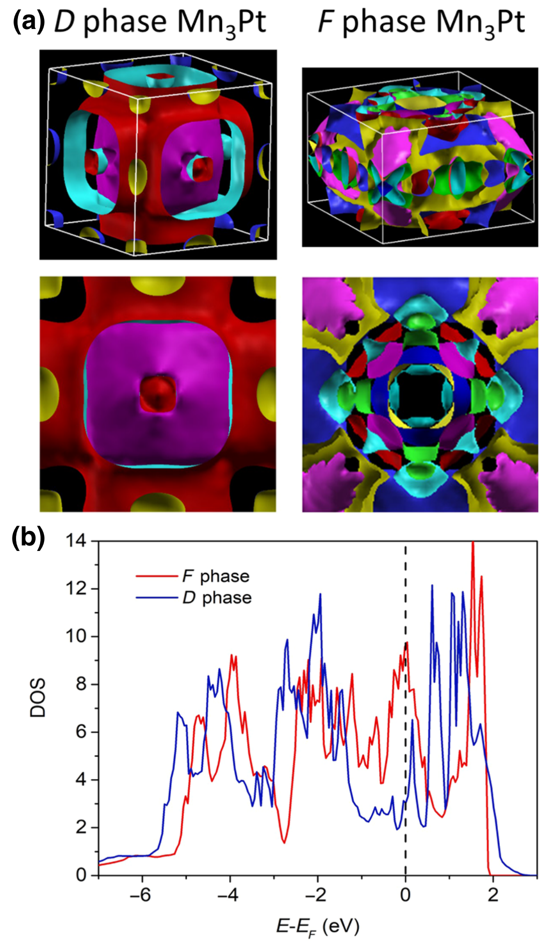

FIG. 2. (a) The side and top views of three-dimensional FSs for Mn_3Pt in D and F phases. The FSs are visualized by using the Xcrysden package [35]. (b) Density of states (DOS) of bulk Mn_3Pt per formula cell for F (red) and D (blue) phases. The Fermi energy lies at zero as indicated by the vertical black dash line.

and the noteworthy difference of the two AFM phases is that there is no available Bloch state around the zone center for the F phase while several Bloch states are present for the D phase, which is evident from the top views shown in Fig. 2(a). This is one of the main reasons for the different transmissions in Mn_3Pt-based MTJs and the resultant large magnetoresistance through the $SrTiO_3$ barrier as we discuss later. The corresponding density of states for the D phase and the F phase are shown in Fig. 2(b). At Fermi energy, the F phase has a relatively larger density of states than the D phase Mn_3Pt.

A $Mn_3Pt/SrTiO_3/Pt$ MTJ is built and shown in Fig. 3(a). The tunnel junction consists of a semi-infinite Mn_3Pt electrode and a $SrTiO_3$ tunnel barrier with a thickness of two unit cells (u.c.) stacked along the [001] direction. Perovskite oxide $SrTiO_3$ with a lattice constant of 3.905 Å is chosen as the tunnel barrier by considering its small lattice mismatch (<1.0%) with Mn_3Pt.

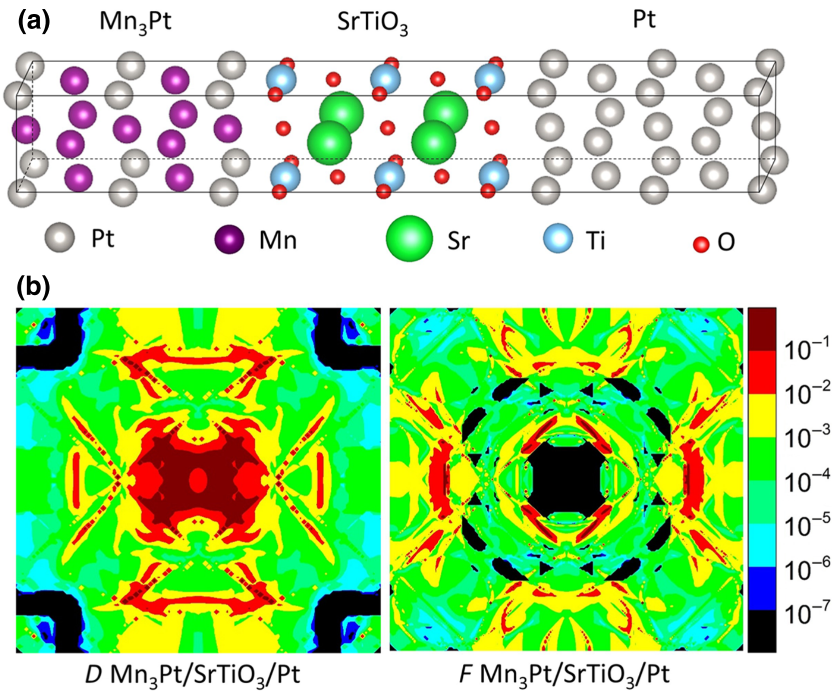

FIG. 3. (a) The side view of the atomic structure of $Mn_3Pt/SrTiO_3/Pt$ tunnel junction. (b) The electron transmission of $Mn_3Pt/SrTiO_3/Pt$ MTJ with Mn_3Pt in D (left) and F (right) AFM phases, respectively. The color bar shows the intensity of transmission.

In addition, Pt with a lattice constant of 3.916 Å [36] serves as a counter electrode, which receives tunneling electrons from the Mn_3Pt electrode. Therefore, the whole $Mn_3Pt/SrTiO_3/Pt$ tunnel junction may be grown epitaxially with a small lattice mismatch. The epitaxial relation between Mn_3Pt and $SrTiO_3$ might be $Mn_3Pt(100)[001]||$ $SrTiO_3(100)[001]||$ Pt[001] with the Ti atoms sitting at the top of the Mn atoms. In the junction, the left lead consists of repeating unit cells of Mn_3Pt and terminates on both ends with a Mn-Pt atomic layer. The $SrTiO_3$ layer is terminated on both sides with a TiO_2 atomic plane. The oxygen atoms are connected with Mn and Pt atoms at the interface, which is energy favorable [16].

The main results of the transport calculation are shown in Fig. 3(b), which displays the $k_{||}$ resolved transmission for the junction with the Mn_3Pt electrode in the D and F phases. In the junction with the D phase Mn_3Pt, an area has the largest transmission of 10^{-1} distributed around the 2DBZ center. In contrast, the FS of Mn_3Pt in the F phase viewed along the [001] direction has holes in the zone center. There are no bulk states in both spin channels of the F phase Mn_3Pt, which results in zero transmission around this area. Accordingly, the total transmission of the $Mn_3Pt/SrTiO_3/Pt$ junction with a D phase Mn_3Pt electrode is relatively larger than that with the F phase Mn_3Pt electrode. When the electric field is applied across the piezoelectric substrate, the Mn_3Pt electrode undergoes a phase transition from the F phase to the D phase. Consequently, the tunneling junction undergoes a transition from a high-resistance state to a low-resistance state. The optimistic MPT TMR can be defined as

$$\text{MPT TMR} = \frac{G_{D\text{ phase}} - G_{F\text{ phase}}}{\min(G_{F\text{ phase}}, G_{D\text{ phase}})} \times 100\%.$$

The electron transmission and the corresponding MPT TMR are listed in Table I. One can see that the MPT TMR is over 500% by this definition.

TABLE I. The electron transmission of $D\text{Mn}_3\text{Pt}$ and $F\text{Mn}_3\text{Pt}$ per formula cell.[a]

	Transmission for $D\text{Mn}_3\text{Pt}$	Transmission for $F\text{Mn}_3\text{Pt}$	Transmission for $P\text{Mn}_3\text{Pt}$	MPT TMR
Bulk Mn_3Pt	0.85	1.87	—	−120%
$Mn_3Pt/SrTiO_3/Pt$	2.5×10^{-2}	0.40×10^{-2}	0.90×10^{-2}	525%
$Mn_3Pt/AlO_x/Pt$	—	—	—	−200%[b]

The transmission of MTJ with paramagnetic Mn_3Pt ($P\text{Mn}_3\text{Pt}$) electrode has also been listed for comparison.
[a]For $F\text{Mn}_3\text{Pt}$, the transmissions for the two spin channels are identical and for noncollinear $D\text{Mn}_3\text{Pt}$, the transmissions of the two spin channels are indistinguishable.
[b]Estimated from density of states at Fermi energy.

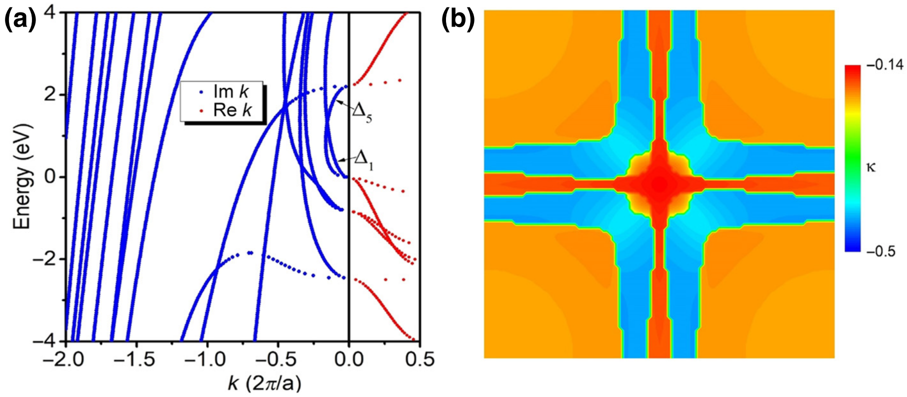

FIG. 4. (a) The complex band structure of $SrTiO_3$ along the [001] direction ($k_{||} = 0$). The real band and the imaginary band are plotted in red and blue, respectively. The top of the valence band is located at zero energy. (b) The two-dimensional complex band dispersion of $SrTiO_3$ at the middle of the band gap with the smallest imaginary part κ (in the unit of $2\pi/a$).

The large MPT TMR in the $Mn_3Pt/SrTiO_3/Pt$ tunnel junction also partly relies on a symmetry selective filtering effect in the $SrTiO_3$ tunnel barrier. As is shown in Fig. 4(a), similar to the band symmetry filtering effect in MgO [1] and spinel oxide $MgAl_2O_4$ [37], the Bloch state with Δ_1 and Δ_5 symmetry has the smallest decay rate within the band gap of $SrTiO_3$. As a consequence, the Bloch states around the Γ point (zone center) may have a relatively larger tunneling possibility. Figure 4(b) shows a complex wave vector with the smallest imaginary part over the entire 2DBZ. It is clear that the slowest electron decay rate forms a cross shape around the Γ point. By comparing the FSs of DMn$_3$Pt and FMn$_3$Pt shown in Fig. 2(a), there is no available Bloch state of FMn$_3$Pt around the Γ point while available Bloch states are present for DMn$_3$Pt. In consequence, for the DMn$_3$Pt/SrTiO$_3$/Pt tunnel junction, because of the large transmission contribution from the Brillion zone center, the tunneling conductance should be much larger than that of the FMn$_3$Pt/SrTiO$_3$/Pt MTJ and should lead to a large positive MPT TMR.

It is worthwhile pointing out that $SrTiO_3$ may not be the unique tunnel barrier material suitable for the proposed tunnel junctions with a Mn_3Pt electrode. Despite the large MPT TMR in the single-crystalline tunnel junction with the $SrTiO_3$ barrier, it is also possible to fabricate a similar junction but with an amorphous barrier, for instance, an AlO_x barrier. By ignoring the difference of tunneling ability of each Bloch state, the electron transmission (or conductance) at zero bias is proportional to the density of states at the Fermi energy of the two electrodes as $T \propto D_{\mathrm{Pt}}(E_F)D_{\mathrm{Mn_3Pt}}(E_F)$. A simple estimation of the MPT TMR with an amorphous AlO_x barrier according to the density of states of FMn$_3$Pt and DMn$_3$Pt shown in Fig. 2(b) is around −200% as it is listed in Table I. Here, the negative sign indicates a larger conductance of FMn$_3$Pt/AlO$_x$/Pt than of DMn$_3$Pt/AlO$_x$/Pt MTJ.

The interfacial magnetic structure may be important for the spin-dependent transport and the resultant TMR in a MTJ [38]. In order to elucidate the effect of possible interface magnetic disorder, additional calculations are performed. Take the FMn$_3$Pt/SrTiO$_3$/Pt-MTJ, for example, where instead of a perfect AFM interface magnetic structure [shown in Fig. 5(a)], we consider 1 u.c. [shown in Fig. 5(b)] and 4 u.c. (not shown) of paramagnetic Mn_3Pt present at the interface. The resultant electron transmission is listed in Table II. Compared with the perfect AFM-ordered Mn_3Pt interface, the paramagnetic Mn_3Pt present at the interface will lead to additional interface scattering and a decrease of electron transmission. However, the MPT TMR has been largely preserved due to the fact that the MPT TMR mostly originates from the features of the FS of bulk Mn_3Pt, as we discussed previously. These results further confirm that the MPT TMR should be robust against the imperfect interfacial magnetic structure.

In a stoichiometry $Mn_3Pt/BaTiO_3$ system, the electric field control of MPT occurs above room temperature at

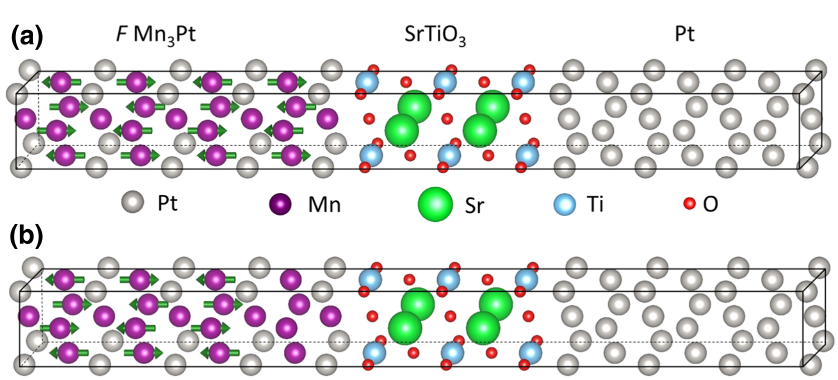

FIG. 5. Atomic structure of FMn$_3$Pt/SrTiO$_3$/Pt MTJ with perfect interface magnetic structure (a) and with 1 u.c. of paramagnetic Mn_3Pt interface (b). The arrows represent the magnetic moments.

TABLE II. The electron transmission of $F\mathrm{Mn_3Pt/SrTiO_3/Pt}$-MTJ per formula cell with different interfacial magnetic structures and the corresponding MPT TMR respective to $D\mathrm{Mn_3Pt/SrTiO_3/Pt}$-MTJ.

Interfacial magnetic structure	Transmission	MPT TMR
1 u.c. $P\mathrm{Mn_3Pt}$	0.11×10^{-2}	+2173%
4 u.c. $P\mathrm{Mn_3Pt}$	0.28×10^{-2}	+793%

around 360 K [22]. It may also be possible to further reduce the MPT temperature to room temperature (300 K) by choosing appropriate materials. For instance, it has been experimentally shown that the MPT temperature of nonstoichiometry $\mathrm{Mn_3PtN}_x$ and $\mathrm{Mn}_{3-x}\mathrm{Pt}_{1+x}$ alloys [25,39,40] can be lowered down to room temperature, and has been theoretically shown that Mn-based antiperovskite nitrides [41] may have a similar AFM phase transition. Instead of a $\mathrm{BaTiO_3}$ substrate, an alternative piezoelectric substrate with a larger piezoelectric effect, for example, a PMN-PT [$\mathrm{Pb(Mg1/3Nb_{2/3})O_3}$-$\mathrm{PbTiO_3}$] [42] substrate may lead to a MPT at room temperature.

Moreover, the electronic structures of $\mathrm{Mn_3Pt}$ in the noncollinear AFM D phase and collinear AFM F phase are significantly different and may lead to other different intrinsic physical properties beyond the magnetoresistance effect in the studied $\mathrm{Mn_3Pt}$-based MTJs. For example, it has been experimentally demonstrated that the noncollinear AFM D phase has moderate anomalous Hall conductivity (AHE) while the collinear AFM F phase has zero AHE conductivity [22]. Thus, one may expect a different spin Hall conductivity (or spin Hall angle) of $\mathrm{Mn_3Pt}$ in two different AFM phases [43]. In addition, noncollinear and collinear AFM $\mathrm{Mn_3Pt}$ may lead to a different exchange bias effect in a $\mathrm{Mn_3Pt}$/FM metal bilayer system. All of these physical properties can be controlled by an electric field through the inverse piezoelectric effect [22,44,45] and can be used in AFM spintronics [23,24].

IV. SUMMARY

In summary, by employing first-principles calculations, we investigate the transport properties of MTJs by using an AFM electrode $\mathrm{Mn_3Pt}$, which can be transformed from a collinear AFM F phase to a noncollinear AFM D phase by applying an electric field across the piezoelectric substrate. Our results show that the magnetoresistance ratio in a $\mathrm{Mn_3Pt/SrTiO_3/Pt}$ tunnel junction can reach hundreds of percentages, making it promising for applications in low-power consumption memory devices. The MPT TMR in the proposed single crystalline MTJ originates from the cooperative effect of different Fermi surfaces of $\mathrm{Mn_3Pt}$ in two AFM phases and the band symmetry filtering effect of the $\mathrm{SrTiO_3}$ barrier. This would make the MPT TMR robust against the possible interface magnetic structure disorder. In addition, by estimating from the density of states, a similar tunnel junction with an amorphous AlO_x barrier also has a large MPT TMR. Such an electric-field-controlled MPT TMR effect is expected in a class of similar materials beyond $\mathrm{Mn_3Pt}$. Moreover, the electric-field-controlled MPT of $\mathrm{Mn_3Pt}$ can be largely extended to other electric controlled phenomena beyond MPT TMR including anomalous Hall, spin Hall, exchange bias, and so on. This work may stimulate future experimental investigations on the MPT TMR mechanism and the application of $\mathrm{Mn_3Pt}$ and similar materials in AFM spintronics.

ACKNOWLEDGMENTS

Jia Zhang and Long You are supported by the National Natural Science Foundation of China with Grants No. 11704135, No. 61674062, and No. 61821003. The calculations in this work are partly performed at National Supercomputer Center in Tianjin, TianHe-1(A) China.

[1] W. H. Butler, X.-G. Zhang, T. C. Schulthess, and J. M. MacLaren, Spin-dependent tunneling conductance of Fe/MgO/Fe sandwiches, Phys. Rev. B **63**, 054416 (2001).

[2] S. S. P. Parkin, C. Kaiser, A. Panchula, P. M. Rice, B. Hughes, M. Samant, and S.-H. Yang, Giant tunneling magnetoresistance at room temperature with MgO(001) tunnel barriers, Nat. Mater. **3**, 862 (2004).

[3] S. Yuasa, T. Nagahama, A. Fukushima, Y. Suzuki, and K. Ando, Giant room-temperature magnetoresistance in single-crystal Fe/MgO/Fe magnetic tunnel junctions, Nat. Mater. **3**, 868 (2004).

[4] J. C. Slonczewski, Current-driven excitation of magnetic multilayers, J. Magn. Magn. Mater. **159**, L1 (1996).

[5] L. Berger, Emission of spin waves by a magnetic multilayer traversed by a current, Phys. Rev. B **54**, 9353 (1996).

[6] Z. Diao, Z. Li, S. Wang, Y. Ding, A. Panchula, E. Chen, L.-C. Wang, and Y. Huai, Spin-transfer torque switching in magnetic tunnel junctions and spin-transfer torque random access memory, J. Phys.: Condens. Matter **19**, 165209 (2007).

[7] L. Liu, C.-F. Pai, Y. Li, H. W. Tseng, D. C. Ralph, and R. A. Buhrman, Spin-torque switching with the giant spin hall effect of tantalum, Science **336**, 555 (2012).

[8] C.-F. Pai, L. Liu, Y. Li, H. W. Tseng, D. C. Ralph, and R. A. Buhrman, Spin transfer torque devices utilizing the giant spin Hall effect of tungsten, Appl. Phys. Lett. **101**, 122404 (2012).

[9] A. Brataas, A. D. Kent, and H. Ohno, Current-induced torques in magnetic materials, Nat. Mater. **11**, 372 (2012).

[10] W.-G. Wang, M. Li, S. Hageman, and C. L. Chien, Electric-field-assisted switching in magnetic tunnel junctions, Nat. Mater. **11**, 64 (2012).

[11] Y. Shiota, T. Nozaki, F. Bonell, S. Murakami, T. Shinjo, and Y. Suzuki, Induction of coherent magnetization switching in a few atomic layers of FeCo using voltage pulses, Nat. Mater. **11**, 39–43 (2012).

[12] F. Matsukura, Y. Tokura, and H. Ohno, Control of magnetism by electric fields, Nat. Nanotech. **10**, 209 (2015).

[13] E. Y. Tsymbal, Electric toggling of magnets, Nat. Mater. **11**, 12 (2012).

[14] E. Y. Tsymbal and H. Kohlstedt, Tunneling across a ferroelectric, Science **313**, 181 (2006).

[15] J. P. Velev, C-G. Duan, J. D. Burton, A. Smogunov, M. K. Niranjan, E. Tosatti, S. S. Jaswal, and E. Y. Tsymbal, Magnetic tunnel junctions with ferroelectric barriers: Prediction of four resistance states from First Principles, Nano. Lett. **9**, 1 (2009).

[16] J. P. Velev, C. G. Duan, K. D. Belashchenko, S. S. Jaswal, and E. Y. Tsymbal, Effect of Ferroelectricity on Electron Transport in $Pt/BaTiO_3/Pt$ Tunnel Junctions, Phys. Rev. Lett. **98**, 137201 (2007).

[17] G. Gerra, A. K. Tagantsev, N. Setter, and K. Parlinski, Ionic Polarizability of Conductive Metal Oxide and Critical Thickness for Ferroelectricity in $BaTiO_3$, Phys. Rev. Lett. **96**, 107603 (2006).

[18] X. Z. Chen, J. F. Feng, Z. C. Wang, J. Zhang, X. Y. Zhong, C. Song, L. Jin, B. Zhang, F. Li, M. Jiang, Y. Z. Tan, X. J. Zhou, G. Y. Shi, X. F. Zhou, X. D. Han, S. C. Mao, Y. H. Chen, X. F. Han, and F. Pan, Tunneling anisotropic magnetoresistance driven by magnetic phase transition, Nat. Commun. **8**, 449 (2017).

[19] J. Zhang, X. Z. Chen, C. Song, J. F. Feng, H. X. Wei, and J.-T. Lü, Giant Tunnel Magnetoresistance with a Single Magnetic Phase-Transition Electrode, Phys. Rev. Appl. **9**, 044034 (2018).

[20] E. Krén, G. Kádár, L. Pál, and P. Szabó, Investigation of the first-order magnetic transformation in Mn_3Pt, J. Appl. Phys. **38**, 1265 (1967).

[21] E. Krén, G. Kádár, L. Pál, J. Sólyom, P. Szabó, and T. Tarnóczi, Magnetic structures and exchange interactions in the Mn-Pt system, Phys. Rev. **171**, 574–585 (1968).

[22] Z. Q. Liu, H. Chen, J. M. Wang, J. H. Liu, K. Wang, Z. X. Feng, H. Yan, X. R. Wang, C. B. Jiang, J. M. D. Coey, and A. H. MacDonald, Electrical switching of the topological anomalous Hall effect in a non-collinear antiferromagnet above room temperature, Nat. Electron. **1**, 172–177 (2018).

[23] V. Baltz, A. Manchon, M. Tsoi, T. Moriyama, T. Ono, and Y. Tserkovnyak, Antiferromagnetic spintronics, Rev. Mod. Phys. **90**, 015005 (2018).

[24] T. Jungwirth, X. Marti, P. Wadley, and J. Wunderlich, Antiferromagnetic spintronics, Nat. Nanotech. **11**, 231 (2016).

[25] H. Yasui, T. Kaneko, H. Yoshida, S. Abe, K. Kamigaki and N. Mori, Pressure dependence of magnetic transition temperatures and lattice parameter, J. Phys. Soc. Jpn. **56**, 12 (1987).

[26] E. Mendive-Tapia and J. B. Staunton, Ab initio theory of the Gibbs free energy and a hierarchy of local moment correlation functions in itinerant electron systems: The magnetism of the Mn_3A materials class, Phys. Rev. B **99**, 144424 (2019).

[27] B. G. Park, J. Wunderlich, X. Martí, V. Holý, Y. Kurosaki, M. Yamada, H. Yamamoto, A. Nishide, J. Hayakawa, H. Takahashi, A. B. Shick, and T. Jungwirth, A spin-valve-like magnetoresistance of an antiferromagnet-based tunnel junction, Nat. Mater. **10**, 347 (2011).

[28] Y. Y. Wang, C. Song, B. Cui, G. Y. Wang, F. Zeng, and F. Pan, Room-Temperature Perpendicular Exchange Coupling and Tunneling Anisotropic Magnetoresistance in an Antiferromagnet-Based Tunnel Junction, Phys. Rev. Lett. **109**, 137201 (2012).

[29] H. Yan, Z. Feng, S. Shang, X. Wang, Z. Hu, J. Wang, Z. Zhu, H. Wang, Z. Chen, H. Hua, W. Lu, J. Wang, P. Qin, H. Guo, X. Zhou, Z. Leng, Z. Liu, C. Jiang, M. Coey, and Z. Liu, A piezoelectric, strain-controlled antiferromagnetic memory insensitive to magnetic fields, Nat. Nanotechnol. **14**, 131 (2019).

[30] P. Giannozzi, S. Baroni, N. Bonini, M. Calandra, R. Car, C. Cavazzoni, D. Ceresoli, G. L. Chiarotti, M. Cococcioni, I. Dabo *et. al.*, QUANTUM ESPRESSO: A modular and open-source software project for quantum simulations of materials, J. Phys.: Condens. Matter **21**, 395502 (2009).

[31] J. P. Perdew, K. Burke, and M. Ernzerhof, Generalized Gradient Approximation Made Simple. Phys. Rev. Lett. **77**, 3865 (1996).

[32] D. Vanderbilt, Soft self-consistent pseudopotentials in a generalized eigenvalue formalism, Phys. Rev. B **41**, 7892 (1990).

[33] Y. Kota, H. Tsuchiura, and A. Sakuma, Ab-Initio study on the magnetic structures in the ordered Mn_3Pt alloy, IEEE. Trans. On. Mag. **44**, 3131 (2008).

[34] A. Smogunov, A. D. Corso, and E. Tosatti, Ballistic conductance of magnetic Co and Ni nanowires with ultrasoft pseudopotentials, Phys. Rev. B **70**, 045417 (2004).

[35] http://www.xcrysden.org/.

[36] P. Haas, F. Tran, and P. Blaha, Calculation of the lattice constant of solids with semilocal functionals, Phys. Rev. B **79**, 085104 (2009).

[37] J. Zhang, X.-G. Zhang, and X. F. Han, Spinel oxides: Δ_1 spin-filter barrier for a class of magnetic tunnel junctions, Appl. Phys. Lett. **100**, 222401 (2012).

[38] J. Zhang, Y. Wang, X.-G. Zhang, and X. F. Han, Inverse and oscillatory magnetoresistance in Fe/MgO/Cr/Fe magnetic tunnel junctions, Phys. Rev. B **82**, 134449 (2010).

[39] E. Krén, E. Zsoldos, M. Barberon, and R. Fruchart, Magnetic properties of the Mn_3PtN_x system, Solid State Commun. **9**, 27–31 (1971).

[40] E. Krén, G. Kádár, L. Pál, J. Sólyom, and P. Szabó, Magnetic structures and magnetic transformations in ordered Mn_3(Rh, Pt) alloys, Phys. Lett. **20**, 331 (1966).

[41] J. Zemen, E. Mendive-Tapia, Z. Gercsi, R. Banerjee, J. B. Staunton, and K. G. Sandeman, Frustrated magnetism and caloric effects in Mn-based antiperovskite nitrides: *Ab initio* theory, Phys. Rev. B **95**, 184438 (2017).

[42] S. Park and T. R. Shrout, Ultrahigh strain and piezoelectric behavior in relaxor based ferroelectric single crystals, J. Appl. Phys. **82**, 1804 (1997).

[43] W. Zhang, M.B. Jungfleisch, W. Jiang, J. E. Pearson, and A. Hoffmann, Spin Hall Effects in Metallic Antiferromagnets, Phys. Rev. Lett. **113**, 196602 (2014).

[44] S. M. Wu, S. A. Cybart, D. Yi, J. M. Parker, R. Ramesh, and R. C. Dynes, Full Electric Control of Exchange Bias, Phys. Rev. Lett. **110**, 067202 (2013).

[45] X. He, Y. Wang, N. Wu, A.N. Caruso, E. Vescovo, K. D. Belashchenko, P. A. Dowben, and C. Binek, Robust isothermal electric control of exchange bias at room temperature, Nat. Mater. **9**, 579 (2010).